J Ther Eng, Vol. 12, No. 1, pp. 365–384, January, 2026

Journal of Thermal Engineering
Web page info: https://jten.yildiz.edu.tr
DOI: 10.14744/thermal.0001086

Research Article

Magnetohydrodynamic mixed convection within a ventilated cavity crossed by a nanofluid: Effect of the obstacle position

Mourad MODERRES[1,*], Seddik KHERROUBI[1], Abdelkader BOUTRA[2,3], Abdelhakim SETTAR[4], Chaouki Ghenai[5], Djelloul AZZOUZI[1], Hakan F. OZTOP[6]

[1]*Laboratory of Industrial Fluids, Measurements and Application (FIMA) UDBKM, Ain Defla, 44225, Algeria*
[2]*Laboratory of Transport Phenomena, USTHB, BP. 32 El Alia, Algiers, 16111, Algeria*
[3]*Algeria School of Applied Sciences, Algiers, 16001, Algeria*
[4]*INSA Centre Val de Loire, University of Orleans, PRISME EA, Bourges, 4229, France*
[5]*Department of Sustainable and Renewable Energy Engineering, College of Engineering, University of Sharjah, Sharjah, 00000, United Arab Emirates*
[6]*Department of Mechanical Engineering, Faculty of Technology, Fırat University, Elazıg, 23119, Turkiye*

ARTICLE INFO

Article history
Received: 11 October 2024
Revised: 09 January 2025
Accepted: 20 January 2025

Keywords:
Circular Obstacle; Magnetic Field; Mixed Convection; Nanofluids; Ventilated Cavity

ABSTRACT

This study presents a numerical investigation into mixed convection heat transfer within a ventilated square cavity containing a circular obstacle, evaluated under various magnetic field inclination angles. Ventilation is ensured by two fixed openings on the vertical walls of the cavity. Cold Carbon Nanotubes-water nanofluid enters through the opening at the top of the left vertical wall and exits through the opening located at the bottom of the right vertical wall. All four walls of the cavity are maintained at the same temperature, which is higher than that of the incoming nanofluid. The finite volume method, combined with the SIMPLER algorithm for pressure-velocity coupling, was utilized to solve the governing differential equations of the system. The objective was to determine the optimal geometry that offers the best thermal performance with the lowest pressure drop. Key results indicate that increasing the nanoparticle volume fraction from 0% to 6% enhances the average Nusselt number by up to 20.3%, significantly improving heat transfer performance. Similarly, tilting the magnetic field at an angle of 45° minimizes the pressure drop by 12% compared to the baseline case. The optimal obstacle position was identified as the cavity center, balancing heat transfer enhancement with a manageable pressure drop. These findings can be applied to optimize the design of cooling systems in industrial applications such as electronic device cooling, energy storage systems, and heat exchangers, where efficient thermal management and minimal pressure loss are crucial. The research introduces a new application of Carbon Nanotubes-water nanofluid to enhance heat transfer performance, with the added complexity of a magnetic field influencing the flow dynamics.

Cite this article as: Moderres M, Kherroubi S, Boutra A, Settar A, Ghenai C, Azzouzi D. Magnetohydrodynamic mixed convection within a ventilated cavity crossed by a nanofluid: Effect of the obstacle position. J Ther Eng 2026;12(1):365–384.

***Corresponding author.**
*E-mail address: mourad.moderres@univ-dbkm.dz

This paper was recommended for publication in revised form by Editor-in-Chief Ahmet Selim Dalkilic

INTRODUCTION

For companies, it is now imperative to manage the thermal performance adequately because with regards to minimized energy consumption and improved system efficiency not only the durability of the material, but also customer confidence are influenced. One possible solution to enhance the heat transfer rate is the addition of nanoparticles in common fluids like water, ethylene [1], Nanofluids were documented and for the first time, a technologically feasible heat transfer fluid have been introduced as a dispersion of metallic nanoparticles in regular Heat Transfer Fluids that substantially enhances the heat conductivity, reduces pumping power to compensate adverse thermophysical properties by far out weighing limitations related with conventional fluids for energy effective heat transfer applications. Also, bottling of metallic or non-metallic NPs into fluids such as water, oils and ethylene glycol increase in the thermal conductivity coefficient and heat transfer rate [2-5]. In addition, the degree of heat transfer enhancement is strongly dependent on the nanoparticle and host fluid properties, particle volume fraction, particle size, particle shape, Brownian motion and thermophoresis [6-10].

However, with the incorporation of nanoparticles, thermal performance is enhanced and pressure drop is increased, which restricts their application in thermal systems.

For instance, the viscosity behavior of Al_2O_3 –water and ZnO ethyleneglycol nanofluids over that of their respective base fluids is reported to be observed as higher in comparison with the base fluids [11, 12] experimentally studied the pressure drop and heat transfer rate of silver-water nanofluids in a counter-flow heat exchanger. The authors found that the pressure drop increased by 55%, and the heat transfer rate increased by 69 % at a volume concentration of 0.9% compared to the base water [13] investigated the heat transfer and pressure drop in helically coiled tube heat transfer working fluid with Al_2O_3 nanofluids under a turbulent flow condition. The increase in heat transfer coefficients and pressure drop is enhanced with particle concentration. The study of heat transfer and pressure drop in a conical helical tube heat exchanger using MWCNT/water nanofluids was the focus of [14]. Their findings revealed that, in comparison to water, the pressure drop increased by approximately 16%, 30%, and 42% for nanoparticle concentrations of 0.1%, 0.3%, and 0.5%, respectively. In addition, several numerical and experimental studies on different cavity shapes have explored the impact of nanofluids on heat transfer and pressure drop performance under different flow regimes [15-18]. All the mentioned studies showed a significant improvement in heat transfer, using nanofluids as working fluid in which the pressure drop also increased.

Over the last decade, a review of literature suggests that researchers have also explored the convective flow of fluids – nanofluids or base fluids filled in cavities with obstacles. It is a very promising solution for an improved thermal performance. For example, [19] performed a numerical investigation of the effect of a square conductive obstacle placed in the center of a square cavity under natural convection. The heat-exchange coefficient has been found to be increased (decreased) by the incorporation of a body with thermal conductance lower (higher) than that of the unit.

Numerically studied the influence of an adiabatic obstacle at the center of a differentially heated square cavity on flow and temperature fields [20]. The outcome reveals an optimal size of obstacle yielding a heat transfer enhancement compared to the case in absence of obstacles. [21] conducted a numerical investigation to analyze how dividing a solid block with varying conductivity affects the flow and heat transfer properties within a square cavity. The findings indicate that subdividing the block postpones the initiation of natural convection and diminishes heat transfer. Additionally, the subdivision of solid blocks does not significantly impact heat transfer at elevated Rayleigh numbers, with blocks featuring lower conductivity proving to be more conducive to convective heat transfer. investigated natural convection in a truncated cone containing Cu-water nanofluid for different Rayleigh numbers, wall inclinations and heat source lengths [22]. The results indicate an enhancement in the cooling capability when nanofluids are used, and this is further controlled by both wall angle and power length of heat [23]. Studied the water-Al_2O_3 nanofluids laminar forced convection in a microchannel heat sink, and obtained favorable heat transfer performance through numerical analysis, revealing that better thermal performance is attained with higher nanoparticle volume concentration and Reynolds number for advanced cooling systems.

Provided a comprehensive review of numerical and experimental results from natural laminar convection in enclosures with and without internal bodies, details were provided for the Rayleigh number, shape ratio, relative position of internal bodies, number of inner bodies and inclination angle of cavity or obstacle [24]. The results show that appropriate values of the control parameters can significantly enhance thermal recirculation in an enclosure with inner objects. Thus, due to the presence of bodies, secondary vortices are developed in the cavity and modification on current lines and isotherms occurs. Therefore, [25] considered the heat transfer of Cu-water nanofluid in a lid-driven cavity having conductive solid square cylinder at its center. Their findings showed that with a reducing of Richardson number, the influence of nanoparticle concentration would decrease[26]. Investigated natural convection in a square cavity containing a nanofluid and an adiabatic square block in the center. The authors have demonstrated that the average Nusselt number has been found to increase with an increasing volume fraction of nanoparticles for all Rayleigh numbers, except $Ra = 10^4$.

Similarly, at low Rayleigh numbers, the heat transfer rate decreases as the adiabatic square body size increases. The natural convection in a square cavity with four hot inner circular cylinders was studied by [27], which were arranged at multiple spatial location of rectangular shape. The authors showed that the flow and thermal fields are consistently stable across the range of $10^3 \leqslant$ Ra $\leqslant 10^4$. However, in the Rayleigh range of 10^5 to 10^6, both velocity and temperature fields become unstable due to the placement of cylinders. In addition, the symmetry with regard to the vertical center line is affected by cylinder locations. Another investigation by [28] explored the heat transfer characteristics of a CuO-water nanofluid within a rhombus-shaped cavity, featuring a square cylindrical obstacle at the cavity center under three different conditions (cold, adiabatic, and hot). The results showed that the cold cylinder hinders heat transfer in cavity when compared with isothermal and hot square cylinders.

Similarly, the cavitymodel with openings have attracted much attention from researchers becaused it frequently appears in practical engineering processing , such as cooling/heating systems. This design aims to optimize the configuration of openings for facilitating heat transfer. For instance, [29] investigated the mixed convection of Al_2O_3-water nanofluid within a ventilated enclosure. hey investigated different combinations of outlet locations, Reynolds and Richardson numbers, and nano-particle volume fractions to find a suitable configuration for these systems. This is a framework whereby saturated boiling has the highest possible heat transfer rate and pressure drop from same. Mixed nanofluid convection in a ventilated irregular cavity was also investigated numerically by [30]. The results show that heat transfer is augmented with increasing nanoparticle volume fraction, Richardson and Reynolds numbers, and decreasing the particle size [31]. investigated mixed convection optimization in a ventilated square cavity containing nanofluid. It was observed that an increase in the Richardson and nanoparticle volume fraction results in a reduction of average Nusselt number. Furthermore, the relative distance of inlet port location from bottom wall of cavity 0 and outlet port location from top wall of cavity 0.9H at Re = 0.01 and Φ = 3% is the optimum configuration for heat transfer. Owing to its practical importance, understanding the mixed convection in ventilated cavities is important in a number of technological applications such as solar collectors, building thermal systems, air conditioning and cooling of electronic boards. The modification of heat transfer in cavities due to the inclusion of obstacles, has recently been a subject of enhanced concern. From reviewing the previously conducted works, it is found that the mixed convection have been widely studied in ventilated square enclosure filled with cavity, as there are obstacles inside and fins on the bottom wall acting as agents of disturbance.. For example, [32] conducted a numerical investigation on steady-state mixed convective laminar flow in a ventilated square enclosure where the right vertical wall was heated and featured a thermally conductive solid cylinder. Their results, considering various obstacle positions and Richardson numbers, indicate a significant impact of obstacle location on the heat exchange rate. Similarly, in another study, [33] investigated mixed convection in a ventilated cavity with a centrally positioned solid, heat-generating circular obstacle, exploring a wide range of Richardson, Reynolds, and Prandtl numbers. They conclude that these parameters have a significant impact on the flow and thermal fields, in addition to the heat transfer rate, drag force and average fluid temperature of the cavity.

The effect of the external magnetic field on the heat transfer of the electrically conductive fluid has also received much attention due to various applications in many fields such as crystal growth, microelectronic devices, control of hydrodynamic behavior and heat transfer during crystal growth processes [34, 35]. Thus, an effect of the inclined uniform magnetic field on the natural convection of an electrical conductor (Pr = 0.025) in a rectangular cavity was numerically studied by [36]. The authors reported that the inclination angles of the magnetic field and the cavity aspect ratio play an important role in different Rayleigh numbersfor fluid flow and heat transfer. Namely,the flow structure depends strongly on the magnetic field inclination angle for a large Hartmann number [37]. numerically studied the natural convection in a fillated nanofluid cavity having obstacles of different shapes (circular, square, and diamond) installed under the influence of a uniform magnetic field and uniform heat generation. The cavity was heated from the bottom and cooled from the vertical sides, while the top wall was assumed to be adiabatic;thesidewalltemperatures vary linearly. It is observed that the presence of obstacles deteriorates the heat transfer process, and this is more pronounced with a higher external Rayleigh number compared to the cavity without obstacles at Ra = 10^6. Reduced heat transfer with square and diamond-shaped obstacles than without obstacles is less effective with increasing Hartmann numbers [38]. Examined porous domain modeling under the influence of radiation and Lorentz forces, employing a hybrid nanomaterial and solving equations through CVFEM. Findings indicate that increased permeability thins the boundary layer, while magnetic fields reduce its impact on Nu_{ave}, buoyancy forces enhance thermal gradients [39]. Analyzed the influence of nanomaterials on MHD flow between non-parallel plates using HPM and RK4 methods. It finds that hydraulic boundary layer thickness decreases with higher Reynolds numbers but increases with a larger Hartmann number [40]. Discussed thermal behavior of nanomaterials in various contexts. The study examines Al_2O_3-water nanofluid flow between plates, incorporating Brownian motion and thermal forces, revealing C_f and Nu increase with higher squeeze and Eckert numbers.

Analyzed the MHD free convection flow of Cu /water nanofluid in a square cavity heated from the bottom and cooled by the side walls [41]. The heat transfer rate increases withthe heat source length, nanoparticle volume fraction, and Rayleigh number and a decreasing function of the Hartmann number [42]. Studied the mixed MHD flow convection of Cu/water nanofluid in an open cavity with an isothermal horizontal wall. The authors showed that an increase in the Lorentz force leads to attenuating the circulation zone inside the cavity for a horizontal and inclined magnetic field [43]. investigated the effect of magnetic field directions on the natural convection of CNT-water nanofluid in a cubical cavity. For different Rayleigh numbers and nanoparticle volume fractions, the results indicate that the heat transfer increases with the increase of nanoparticle volume fraction. At the same time,the magnetic force inhibits the heat transfer by 50% when the Hartmann number is increased from 50 to 100. Moreover, the magnetic field angles are more pronounced for Ra $=10^5$ [44]. Numerically examined the natural convection of TiO2-water nanofluid in a cubic cavity containing a hot block under the influence of a magnetic field, emphasizing the effects of 3D flow and the enhancement of heat transfer by nanoparticles. The results indicate that buoyancy enhances heat exchange, while magnetic fields inhibit it, with 3D flows showing significant differences from 2D, particularly at high Rayleigh numbers.

Considered numerically mixed convection in a square cavity with a heated and filled lid of nanofluid alumina-water whose isothermal square blockage inside the magnetic field [45]. For other parameters, the average Nusselt number decreased with an increase in the magnetic field. Numerical analysis of free convection in a square cavity filled with a saturated porous media with liquid gallium subjected to an inclined uniform magnetic field was performed by [46]. The bottom of the enclosure is presumed to be uniformly heated. It is assumed that the top boundary of the horizontal top surface is insulated, whereas the left vertical side of the cavity is subjected to a linear heat generation and the right side wall is linearly heated or cold. It has been found that in the case of a linearly heated right wall, the average Nusselt number is an increasing function of the Darcy number, and the vertical magnetic field results in higher values for the average Nusselt number compared to the horizontal magnetic field along the bottom and sidewalls of the cavity. For the cold right wall case, the horizontal magnetic field leads to higher values of the meanNusselt number than the vertical magnetic field case. The average Nusselt number decreases as one moves along the lower and right. At the same time, it increases along the left wall with increasing distance [47]. Demonstrated the effectiveness of the GMDH-type neural network in modeling heat transfer in MHD nanofluids, outperforming the CVFEM approach. Key findings reveal that heat transfer improves with increased buoyancy, nanoparticle concentration, and enclosure slope but decreases with higher Hartmann numbers. Explored the impact of microrotational velocity and radial magnetic fields on laminar natural convection flow within vertical concentric annuli containing a polar fluid. The results highlight the effects of the Hartmann number, vertex viscosity, and annular gap on parameters such as velocity, induced magnetic fields, and current density [48]. In another study, [49] investigated unsteady heat transfer and entropy generation in a viscoelastic Maxwell fluid subjected to an induced magnetic field over a stretching sheet, employing numerical methods for their analysis. Their key findings highlight the influence of various parameters on velocity, magnetic distribution, thermal boundary layers, and entropy generation.

Recently, [50] have studied the influence of external magnetic field on heat transfer and entropy generation of hybrid nanofluid past a partially heated non-uniform ventilated cavity for different control parameters. They found that the enhancement of magnetic field strength usually has a tendency to resist the convective heat transfer and restrict thermal boundary layer thickness. For the entire range of Ha and Re, the nanoparticles' inclusion enhances the Nusselt number [51]. Analyzed the influence of the position of outlet for various control parameters of a nanofluid, inside a ventilated cavity in the presence of magnetic field. Numerical results indicate that the heat transfer rate is influenced by the location of the outletpoints [52]. Investigated analytically the magnetohydrodynamic free convection with radiation and Hall currents in a porous media between vertical walls. The present investigation focuses on chilled panels for aluminum smelters. They emphasize the important role played by the parameters such as Hartmann number, Hall current and radiation in controlling flow patterns, velocity field and magnetic fields. These observations help to increase the system knowledge before even having a prototype [53].

Presented a study on nanofluid heat transfer inside a porous media with a uniform magnetic field, in which they considered the impact of Rayleigh number, Hartmann number and the properties of nanofluid. Results indicate that on increasing the Rayleigh number and nanoparticles property ratio, heat transfer increases, while is further intensified for a lower Hartmann number [54]. Analyzed an analytically solution of the effects of heat radiation, chemical reaction and induced magnetic field on natural convective MHD flow in a porous medium between vertical walls. Their main results show that the influences of so many parameters are remarkable on the profiles of velocity, temperature and magnetic fields, which may have extensive applications in some chemical reactors and solar thermal systems has studied the application of ferro nanoparticles in screw heat exchangers with focus on influence of variable magnetic fields and geometrical process parameters on enhancement of thermal performance. Computations indicate that Reynolds number has the most effect on the flow of nanofluid, and screw diameter has an important impact on skin friction [55].

Recent research has increasingly examined heat transfer optimization in enclosures containing internal obstacles, under diverse operating conditions such as natural and mixed convection, varying Rayleigh numbers, and the influence of magnetic fields. The originality of the present study stems from:

- Investigating the combined effects of circular obstacle positioning and external magnetic fields on the performance of CNT-water nanofluids within ventilated cavities.
- Optimizing thermal performance while minimizing pressure drops, a balance that has practical applications in thermal management systems such as cooling, air conditioning, and electronic devices.
- Exploring a wider range of control parameters than reported in existing literature, enabling the identification of optimal configurations for energy efficient design.

In this paper we attempt to fill in this gap by carrying out a numerical investigation to establish an optimal combination of obstacle layout and magnetic field arrangement for the maximum heat transfer accompanied by minimal flow resistance.

PROBLEM DESCRIPTION

Figure 1 shows the geometry of the present study. The flow takes place inside a ventilated square cavity of length L and height H (L = H) containing a circular obstacle of diameter D (D = 0.1H) and thermal conductivity k^* which changes place in the cavity: P_1 (X = 0.50, Y = 0.50), P_2 (X = 0.50, Y = 0.75), P_3 (X = 0.75, Y = 0.50), P_4 (X = 0.50, Y = 0.25) and P_5 (X = 0.25, Y = 0.50). The cavity is filled with a nanofluid from two equal cross sectional on some height

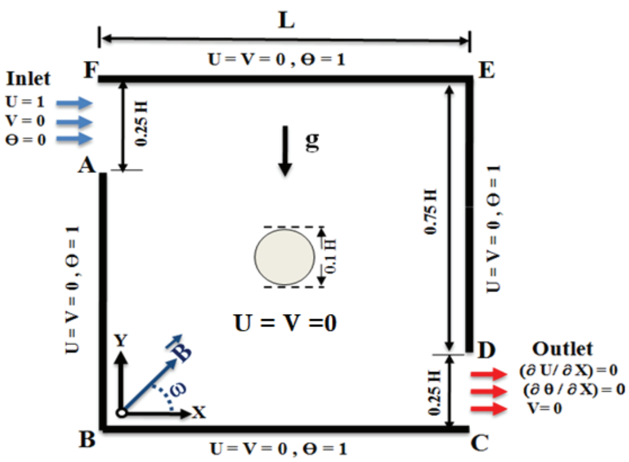

Figure 1. Geometrical representation of the present problem.

(0.25H) at other angles of uniform magnetic field ($\vec{B}$) for the horizontal plane. The cool nanofluid is injected and sucked from the two openings located at the top of the left vertical side and at bottom fo the right vertical side, respectively. All cavity walls are assumed to be isothermal and at the base fluid temperature of the enteringnanofluid. Table. 1 Thermophysical properties of water and CNT nanoparticles are shown in Table 1.

Simplifying Hypotheses

The following assumptions were established:

- The base fluid and the solid spherical nanoparticles are in thermal equilibrium.
- The solid nanoparticles and base fluid are assumed to be in thermal equilibrium.
- The nanofluid is Newtonian and incompressible.
- The Boussinesq approximation is used to determine the density variation in the buoyancy term, where the other thermophysical properties of the nanofluid are assumed constant.
- The flow is considered to be steady, two-dimensional, and laminar.
- The effects of radiation, viscous dissipation, and Joule heating are negligible.
- The induced magnetic field is sufficiently weak to be neglected compared to the applied magnetic field B_0.
- The Hall effect is neglected.

Governing Equations

Given the simplifying hypothesis considered above, the governing equations describing the flow and thermal field used in this study are the continuity, momentum, and energy equations, respectively. The primary assumptions indicate that effects such as radiation, viscous dissipation, Joule heating, the Hall effect, and induced magnetic fields are negligible compared to the applied magnetic field B_0, These equations are defined in their nondimensional forms as follows:

$$\nabla \cdot \vec{V}' = 0 \tag{1}$$

$$\rho_{nf}\,(\vec{V}'\cdot\nabla)\vec{V}' = -\nabla p + \mu_{nf}\,\nabla^2\vec{V}' + (\rho\beta)_{nf}\,(T - T_{Inlet})\vec{g} + (\vec{J}\wedge\vec{B}) \tag{2}$$

$$\vec{V}'\cdot\nabla T = \alpha_{nf}\,\nabla^2 T \tag{3}$$

Table 1. Thermophysical properties of water (Pr = 5) and CNT nanoparticles [43].

	$Cp\,(J\,kg^{-1}\,K^{-1})$	$\rho\,(kg\,m^{-3})$	$k\,(W\,m^{-1}\,K^{-1})$	$\beta\times10^5\,(K^{-1})$
Water	4179	997.1	0.613	21
CNT	650	1350	3500	4.20

where, the applied magnetic field B ($\vec{B} = \vec{B}_X\, i + \vec{B}_Y\, j$) is uniform with a constant magnitude B_0 ($B_0 = \sqrt{B_X^2 + B_Y^2}$)

The interaction between electromagnetic fields and the electrically-conducting nanofluid flow constitutes the Lorentz force [51, 56, 57]:

$$\vec{F} = \vec{J} \wedge \vec{B} \tag{4}$$

The electric current density is governed by the generalized Ohm's law, defined as follows [42-44]:

$$\vec{J} = \sigma_{nf}\left[\vec{E} + \left(\vec{V}' \wedge \vec{B}\right)\right] \tag{5}$$

where, σ_{nf} is the electrical conductivity of the nanofluid, ($\vec{E}$) is the electrical field intensity.

When all cavity walls are electrically insulated [51] and [57]: $\vec{E} = 0$

where, V' ($\vec{V}' = u\,\vec{i} + v\,\vec{j}$) is the velocity vector.

Thus, the expressions of the Lorentz force components are defined for the x and y directions, respectively:

$$\begin{aligned} F_x &= -\sigma_{nf} B_0^2 \sin\omega\left(u\sin\omega - v\cos\omega\right) \text{ and} \\ F_y &= -\sigma_{nf} B_0^2 \cos\omega\left(v\cos\omega - u\sin\omega\right) \end{aligned} \tag{6}$$

The effective density, heat capacity, and thermal expansion coefficient of the nanofluidare respectively:

$$\rho_{nf} = (1-\varphi)\rho_{bf} + \varphi\rho_s \tag{7}$$

$$\left(\rho C_p\right)_{nf} = (1-\varphi)\left(\rho C_p\right)_{bf} + \varphi\left(\rho C_p\right)_s \tag{8}$$

$$(\rho\beta)_{nf} = (1-\varphi)(\rho\beta)_{bf} + \varphi(\rho\beta)_s \tag{9}$$

For the effective thermal conductivity and the effective dynamic viscosity, the formulas used by [29] are, respectively:

$$k_{nf} = \frac{(k_s - k_{lr})\varphi k_{lr}\left(2\beta_1^3 - \beta^3 + 1\right) + (k_s + 2k_{lr})\beta_1^3\left[\varphi\beta^3(k_{lr} - k_{bf}) + k_{bf}\right]}{\beta_1^3(k_s + 2k_{lr}) - (k_s - k_{lr})\varphi\left(\beta_1^3 + \beta^3 - 1\right)} \tag{10}$$

$$\mu_{nf} = \mu_f\left(150\varphi^2 + 2.5\varphi + 1\right) \tag{11}$$

with, $\beta = 1 + (h/a)$; $\beta_1 = 1 + (h/2a)$; $k_{lr} = 2k_{bf}$

where, h is the interfacial layer thickness, a is the particle radius, and lr denotes the layer.

From the work data of [58]: h = 1 nm and a = 10 nm.

The dimensionless form of the governing equations can be obtained by introducing the dimensionless variables as follows:

$$\begin{aligned} &(X, Y) = \frac{(x, y)}{H};\ (U, V) = \frac{(u, v)}{u_{Inlet}};\ \theta = \frac{T - T_{Inlet}}{T_{Wall} - T_{Inlet}}; \\ &P = \frac{p}{\rho_{nf}\, u_{Inlet}^2}\quad Pr = \frac{\nu_{bf}}{\alpha_{bf}};\ Re = \frac{u_{Inlet}\, H}{\nu_{bf}}; \\ &Ha = B_0\, L\left(\frac{\sigma_{nf}}{\mu_{bf}}\right)^{1/2} \end{aligned} \tag{12}$$

After substitution of the above variables, we obtain the following dimensionless equations:

$$\frac{\partial U}{\partial X} + \frac{\partial V}{\partial Y} = 0 \tag{13}$$

$$\begin{aligned} U\frac{\partial U}{\partial X} + V\frac{\partial U}{\partial Y} = &-\frac{\partial P}{\partial X} + \frac{\mu_{nf}}{\rho_{nf}\,\nu_{bf}}\frac{1}{Re}\left(\frac{\partial^2 U}{\partial X^2} + \frac{\partial^2 U}{\partial Y^2}\right) \\ &-\frac{\rho_{bf}\, Ha^2}{\rho_{nf}\, Re_{bf}}\sin\omega\left(U\sin\omega - V\cos\omega\right) \end{aligned} \tag{14}$$

$$\begin{aligned} U\frac{\partial V}{\partial X} + V\frac{\partial V}{\partial Y} = &-\frac{\partial P}{\partial Y} + \frac{\mu_{nf}}{\rho_{nf}\,\nu_{bf}}\frac{1}{Re}\left(\frac{\partial^2 V}{\partial X^2} + \frac{\partial^2 V}{\partial Y^2}\right) + \frac{(\rho\beta)_{nf}}{\rho_{nf}\,\beta_{bf}} Ri\,\theta \\ &-\frac{\rho_{bf}\, Ha^2}{\rho_{nf}\, Re_{bf}}\cos\omega\left(V\cos\omega - U\sin\omega\right) \end{aligned} \tag{15}$$

$$U\frac{\partial \theta}{\partial X} + V\frac{\partial \theta}{\partial Y} = \frac{\alpha_{nf}}{\alpha_{bf}}\frac{1}{Re_{bf}\, Pr}\left(\frac{\partial^2 \theta}{\partial X^2} + \frac{\partial^2 \theta}{\partial Y^2}\right) \tag{16}$$

where, $\alpha_{nf} = k_{nf}/\left(\rho C_p\right)_{nf}$ is the thermal diffusivity of nanofluid and $Ha^2 = \sqrt{\frac{\sigma B^2 L}{\mu}}$ is the Hartmann number,

$Re_{bf} = \frac{\rho_{bf} V L}{\mu_{bf}}$: the Reynolds number for base fluid.

For a solid obstacle, the energy equation is:

$$\left(\frac{\partial^2 \theta^*}{\partial X^2} + \frac{\partial^2 \theta^*}{\partial Y^2}\right) = 0 \tag{17}$$

The boundary conditions are in the following forms:

- **Hot walls:** all walls are assumed to be at a high temperature T=T_H, with no-penetration and no-slip conditions:
- Left wall (x = 0 and 0 ≤ y ≤ 0.75H)
- Right wall (x = L and 0.25H ≤ y ≤ H)
- Top wall (y = H and 0 ≤ x ≤ L)
- Bottom wall (y = 0 and 0 ≤ x ≤ L)
- In dimensionless form: U = V = 0 and θ = 1.
- **Inlet opening:** The inflow is cold (T = T_C) with a uniform velocity u = u_0
- In dimensionless form: U = 1, V = 0 and θ = 0.
- **Outlet opening:** A steady-state regime is assumed.
- In dimensionless form: ∂U/∂X = ∂θ/∂X = 0 and V=0.
- **Obstacle surfaces**: No-slip and no-penetration conditions apply.

- In dimensionless form: U = V = 0.
- **Nanofluid-Obstacle interface**: $(\partial\theta/\partial n)_{nf} = (k^*/k_{nf})(\partial\theta/\partial n)_{Obstacle}$

Heat Transfer and Pressure Drop

To study the heat transfer characteristics related with mixed convection (along the four hot walls), we should consider these variations of local and average Nusselt numbers on the walls, which are as follows:

$$Nu = -\frac{k_{nf}}{k_{bf}}\frac{\partial\theta}{\partial n}\bigg|_{Wall} \tag{18}$$

(n): Normal direction to the considered wall.

The total average Nusselt number is:

$$Nu_{avg} = \frac{1}{4}\left(\frac{1}{AB}\int_A^B Nu\,dY + \frac{1}{BC}\int_B^C Nu\,dX + \frac{1}{DE}\int_D^E Nu\,dY + \frac{1}{EF}\int_E^F Nu\,dX\right) \tag{19}$$

The dimensionless pressure drop is determined from the following equation [29]:

$$C_P = \frac{P_{avg}(\text{Inlet}) - P_{avg}(\text{Outlet})}{(1/2)\,\rho\,u^2_{Inlet}} \tag{20}$$

where,

$$P_{avg}(\text{Inlet}) = \frac{1}{0.25H}\int_A^F P\,dY \quad \text{and} \quad P_{avg}(\text{Outlet}) = \frac{1}{0.25H}\int_C^D P\,dY \tag{21}$$

To estimate heat transfer enhancement between the case of φ = 2% and the base fluid case, EN is defined as follows:

$$EN = \left[\frac{Nu_{avg}(\varphi = 2\%) - Nu_{avg}(\varphi = 0\%)}{Nu_{avg}(\varphi = 0\%)}\right] \times 100 \tag{22}$$

Numerical Method (code validation and grid testing)

We discretized the dimensionless governing equations used in this work by the finite volume method in agreement with [59]. The system of the algebraic equations and boundary conditions was solved using line-by-line technique combined with the TDMA. Moreover, the pressure-velocity coupling was treated using SIMPLER algorithm to guarantee a robust and accurate numerical solution formulation.

The convergence condition used for this study is:

$$\left[\frac{\sum_{i=1}^{L}\sum_{j=1}^{M}\left|\phi_{i,j}^{\xi+1} - \phi_{i,j}^{\xi}\right|}{\sum_{i=1}^{L}\sum_{j=1}^{M}\left|\phi_{i,j}^{\xi+1}\right|}\right] \le 10^{-5} \tag{25}$$

where, L and M are the numbers of grid points in the X and Ydirections, respectively, f is any of the computed field variables and ξ is the iteration number.

In order to validate our numerical code, we compared our results with those obtained in [29] for a Newtonian fluid passing through a ventilated square cavity in terms of the variation of the local Nusselt number measured along the hot walls for Ri = 0, Re = 500 and φ = 0%. Figure 2 shows a very good match. The comparison indicates a good agreement with differences mainly not exceeding 3.76% in high thermal gradient regions. Such variations are attributed to small differences in the boundary conditions and the discretization schemes.

In addition, in the presence of the magnetic field, figure 3 compares the results of [57] Yu in terms of isotherm distribution. Thus, figure 3 shows an excellent resemblance. Finally, the temperature distributions on the horizontal midline were compared with the previous experimental

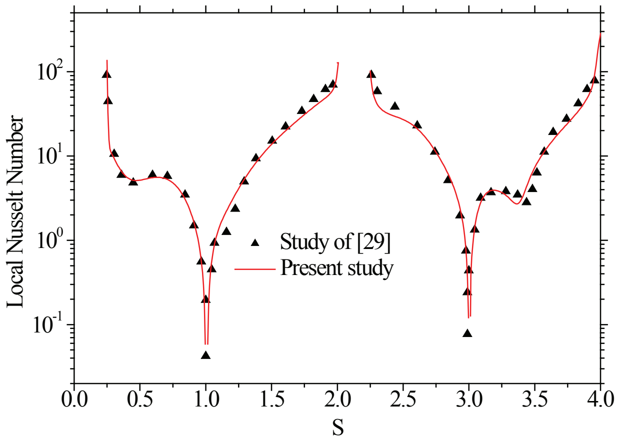

Figure 2. Local Nusselt number on the four walls of the cavity.

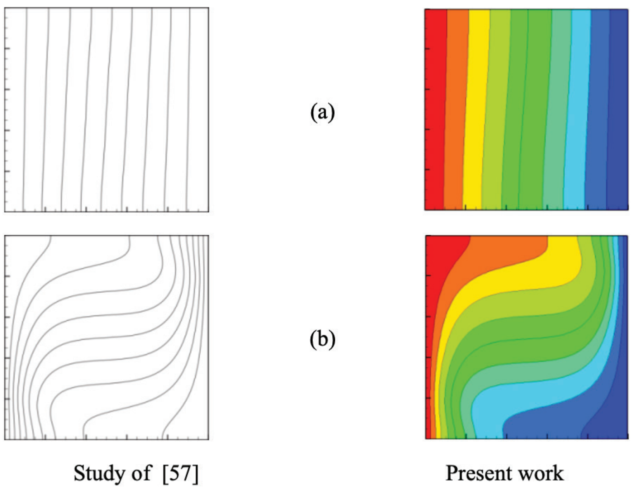

Figure 3. Comparison of isotherms between the present work and study of [57] at $\omega = 0^0$: (a) Ra = 10^4, Ha = 100 and (b) Ra = 10^5, Ha = 30.

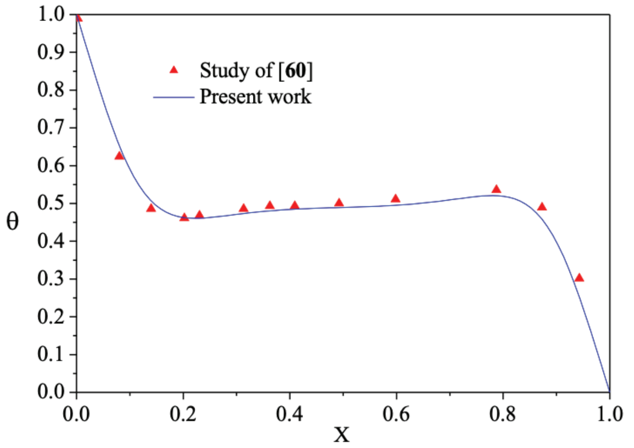

Figure 4. Comparison of the temperature distribution with the experimental results of [60] at Ra = 1.89×10^5 and Pr = 0.71.

results of [60] (Fig. 4), differences of about 2.14% are observed at certain position on the horizontal midline, in particular near steep temperature gradient areas just to the right of the highly underexpanded regime. These may be related to variation in the experimental configuration and assumptions about flow properties.

For the grid generation, we took a mixed convection flow in a ventilated square cavity for Re = 500, Ha = 100. φ = 2% and ω = 90^0 with the circular obstacle in the middle of the cavity P_1. Various grid sizes (120^2 - 220^2) were studied. The results in Fig. 5 indicated that a grid of size 2002 is acceptable for the present analysis. It is important to mention that mesh inflation was not performed at the boundary layer, thus keeping a uniform mesh distribution in all over the domain.

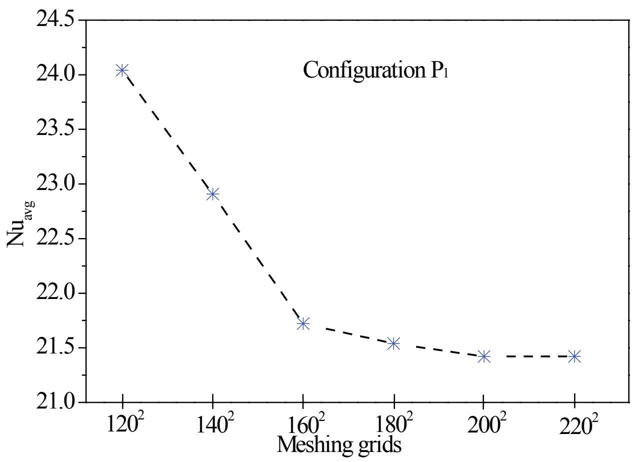

Figure 5. Average Nusselt number versus grid sizes. Ri = 1, Re = 500, Ha = 100, ω = 90° and φ = 2%.

RESULTS AND DISCUSSION

The effect of the obstacle position, Table. 2, in a ventilated cavity filled with an electrically conductive nanofluid based on water and nanoparticles (φ = 2%) under the action of a magnetic field is numerically studied in mixed convection mode. The objective is to determine the best position of the obstacle corresponding to the maximum heat transfer rate and minimum pressure drop as a function of the different control parameters: Reynolds number, Hartmann number, magnetic field direction, and the volume fraction of the nanoparticles (φ = 2%).

Table 2. Obstacle positions in the ventilated cavity

Obstacle position	(x, y)
P_1	(0.5, 0.5)
P_2	(0.5, 0.75)
P_3	(0.75, 0.5)
P_4	(0.5, 0.25)
P_5	(0.25, 0.5)

Hydrodynamic and Thermal Field

At Ha = 0, the streamline and isotherm are presentedin Fig. 6. When Re is small (Re = 50), the typical structure of the streamlines consists of two rotating cells. One is on the right side of the top wall and rotating counter clockwise, and another larger cells are also rotating but clock-wise near the left wall for each configuration. The state P_5 is identified by the emergence of a third rotating cell at the inlet. Indeed, for the high Reynolds number (Re = 500) the amplification of rotating cells and a clear observation of secondary cells above the obstacle is noted for P_1, P_2 and P_3 configurations. This is due to the presence of anobstacle in the main flow.

In addition, we observe that the repositioning of the obstacle leads to traffic flow-line rearrangement (also for public transportation lines and routes). This influenceis manifested through the change, in size and shape, of the rotating cells and by that on the exchange in the parietal zone of fluid across between walls. For example, as Re = 50 in figure 1, by changing the location of the obstacle from P_1 to P_2, the rotating cells become larger. In fact, when the magnitude of the inertial force is large (Re = 500), in the main flow linking both vent positions we can see a very remarkable change when obstacle is located at P_2 and P_3. This is due to the interaction of the obstacle Wake with main flow. It is, indeed, because the expanding rotating cells along with its core (Figs 3c and 3d) are better developed when the obstacle's position is at the core of the rotating cell in bottom cavity (see configurations P_4 and P_5). As for the isotherms described in Fig. 6b, it is possible to observe the behaviour of the streamline versus Re on top of the isotherms shape. It is true that the thickness of thermal boundary layer decreases with increasing Reynolds number. The obstruction position does, on the other hand, have a major impact on the progress of the boundary layer thickness. The P_2 and P_3 have the smallest thickness among the other Re = 500.

We demonstrate that the interaction of the main flow with the obstacle causes to change in main flow and streamline distribution. This effect (restriction) is reflected in the size and shape of the circulating cells, and thus on blood-fluid exchange cross-diuse between wall to circulating particles. For instance, at Re = 50 the removal of same to after having introduced it allove a growth of around the rotating cells. In fact, in the stronger intensity of the inertial force case (500), a significant change takes place at this main flow connecting the throat positions for and when Re = 50. This result can be ascribed to the interaction between main flow and the obstacle. Hence, the expansion of rotating cells is expected to occur when the obstacle occupies the center of the rotating cell at bottom confining wall (cases and). With respect to the isotherms, in Figure 6b we demonstrate isotherm configuration development of the streamline with Reynolds. The thermal boundary layer thickness is actually decreased with Re. Sensitivity to the obstacle position The boundary-layer thickness growth is, however, strongly dependent on the obstacle position. The two thinnest configurations among all the Re = 500 cases are P_1 and P_2.

Figures 7 and 8 show the magnetic field effects for Re = 500 and different magnetic field inclination angles at

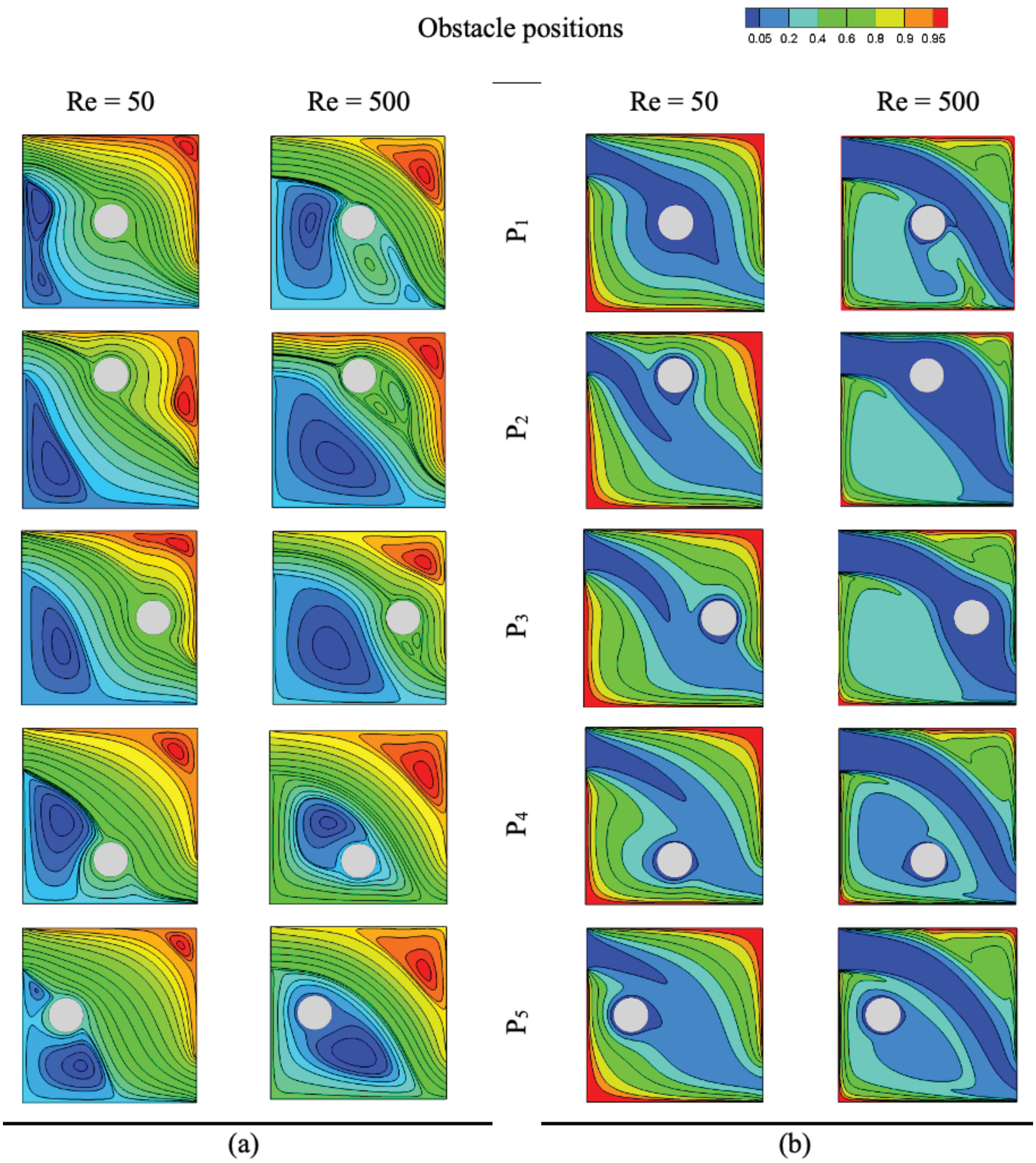

Figure 6. Effect obstacle position versus Re on streamlines (a) and isotherms (b) for Ha = 0 and φ = 2%.

Ha = 100. These effects correspond to the obstacle's position on the streamlines and the isothermal distributions for the nanofluid (φ = 2%), respectively. First, we compared the impact of the magnetic field direction as a function of the variation of the obstacle position compared to the case of the absence of the magnetic field (Fig. 6). For ω = 0° and ω = 45°, we notice that the streamlines are almost similarregardless of the obstacle position. The rotation cells observed in the absence of the magnetic field and streamlines are weakened, tend to disappear close to the active walls and become almost parallel near these walls which correspond to a heat transfer conduction.

In contrast, in the P_2 configuration, the cells located at the bottom do not disappear completely but undergo degradation in size. This is due to the fact that the movement of the flow induced by the inertial forces slows down, and the shear forces become dominant by the applied magnetic field. Indeed, the Lorentz and inertial forces act in the opposite direction (*See the Momentum Equations*). For ω = 90°, this time, we observe the reduction of the rotating cell size localized at the lower cavity and the disappearance of the cell located at the top for all configurations. This findingcan be explained by the fact that the Lorentz force acts this time perpendicular to the main flow direction. For ω = 135°, we note the disappearance of the secondary cells. The cell located at the top amplifies significantly, and the cell's sizeat the bottom decreases. This phenomenon can be explained by the inertia force being stronger than the Lorentz force. Moreover, it can be seen that the effect of inclination angles on the flow structure is considerable significant when ω = 0° and ω = 45° are compared to other angles (ω = 90° and ω = 135°).

Figure 8 illustrates the isotherms, and it can be notedthat the space occupied by the main flow (characterized by the lowest temperature 0.05) is considerably larger in the presence of the magnetic field at different angles, except for the case when the angle is equal to 135°. Thus, the thickness of the boundary layer in the case is ω = 45°. It is the

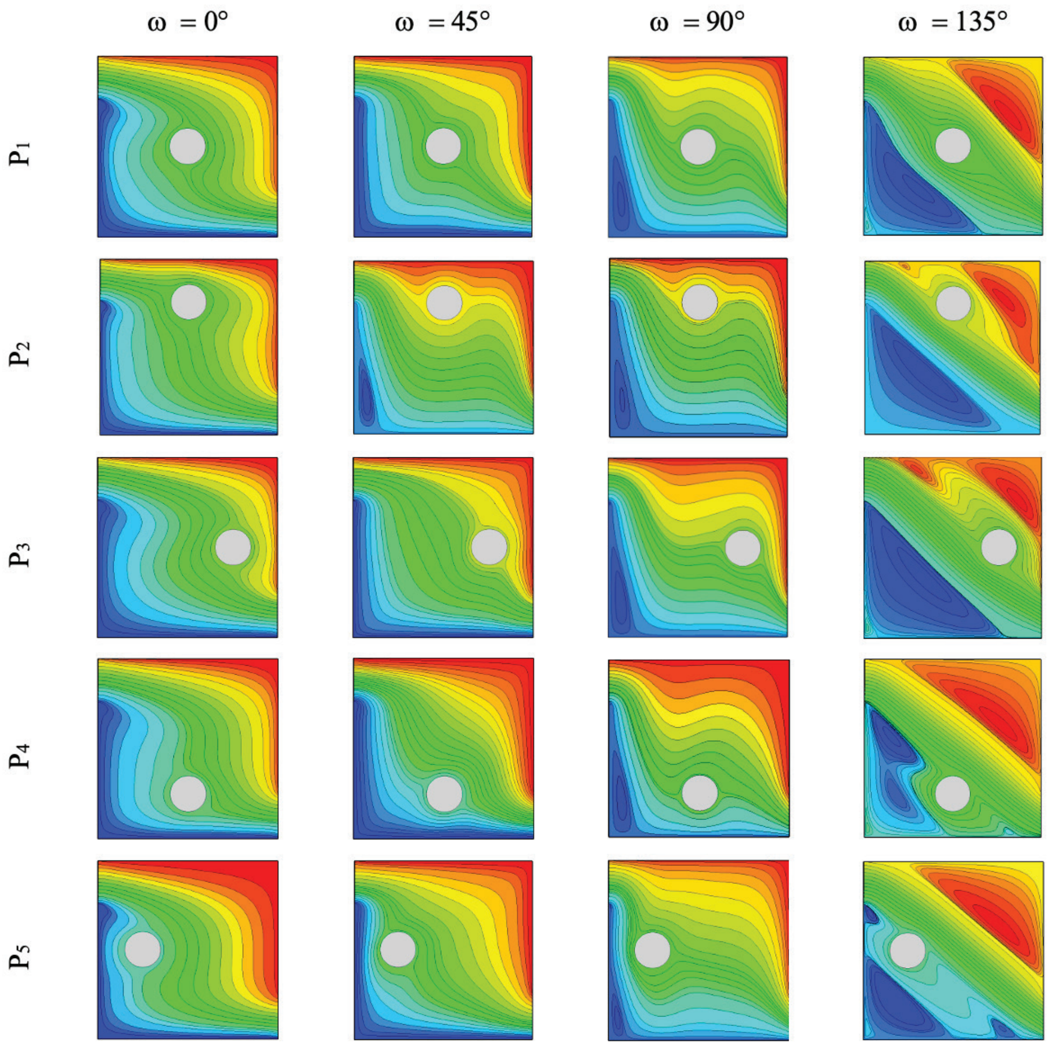

Figure 7. Streamlines versus magnetic field direction for all obstacle positions at Re = 500, Ha = 100 and φ = 2%.

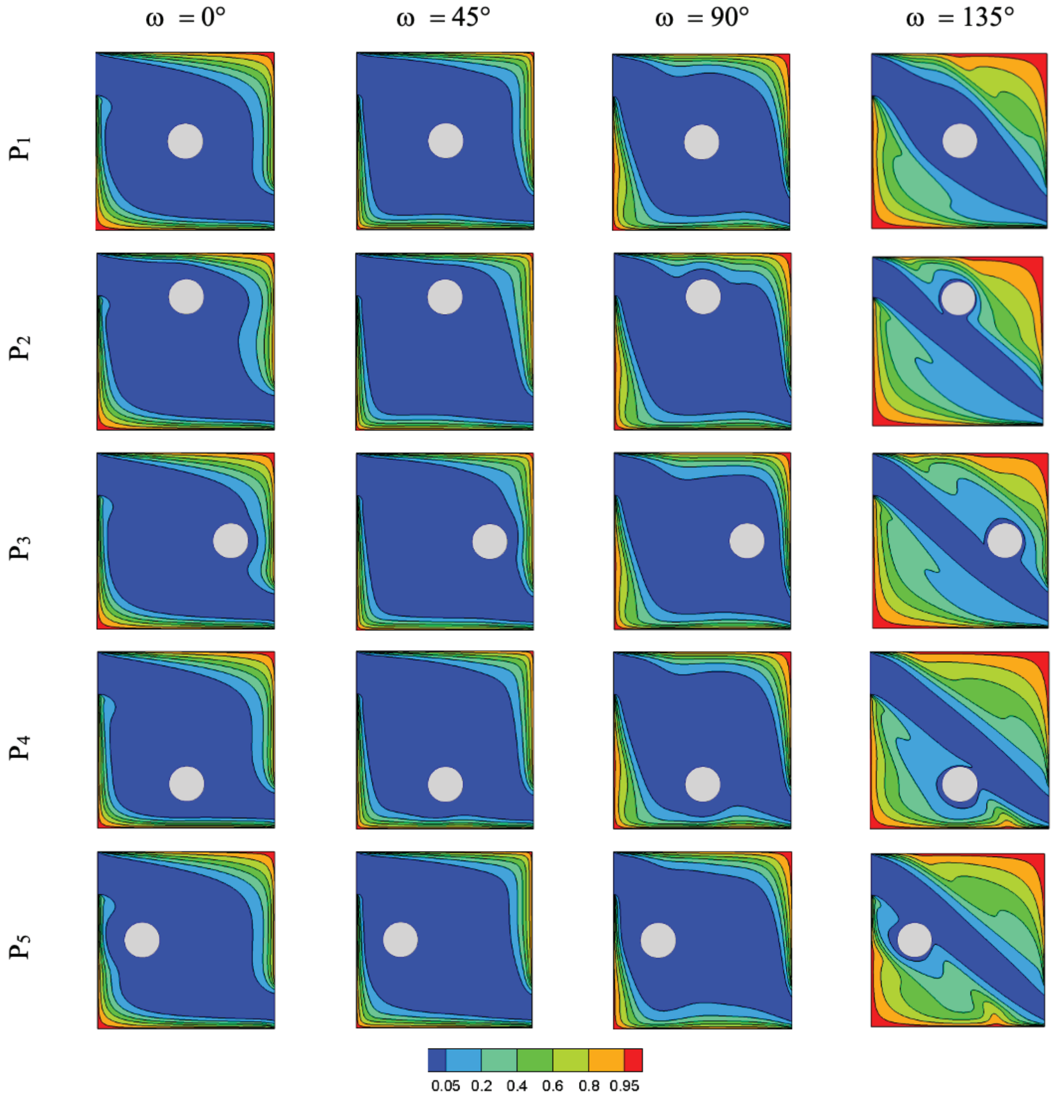

Figure 8. Isotherms versus magnetic field direction for all obstacle positions at Re = 500, Ha =100, and φ = 2%.

thinnestcompared to the cases obtained by the other angles. This means that the parietal exchange (fluid/walls) is very important. Moreover, we observe that the change in the obstacle's position has a remarkable influence on the distribution of the isotherms only for 135°.

Transfer Rates

In this context, to assess the nanofluid-wall heat transfer as a function of magnetic-field orientation, we studied the local Nusselt number characteristics across the hot walls for P_4 configuration at Re = 500, Ha = 100 and φ = 2%. The dimensionless local Nusselt number characterizes convective heat transfer efficiency by account of the thermal gradients and fluid dynamics in the vicinity of walls. Figure 9 that the orientation of the magnetic field heavily affects the heat-transfer process. In particular, for the inclination angle of the magnetic field at 45°, maximum local Nusselt number is found to occur over the hot walls. Such a promotion of the heat transfer by mixed convection may be due to the improved effect of the Lorentz force as well as convective streaming developed in this angle. For the case of field at 450 angle, the magnetic fields are inclined with respect to thermal loading that provide a more effective mixing in nanofluid. This alignment is presumably chosen in the sense to minimize magnetic damping effect to suppress convective flow (a typical phenomenon at larger Hartmann numbers), but still making use of anisotropic field conductive paths.

In contrast, the Nusselt number is smaller when magnetic field angles change from 90° to 135° implying a decrease in heat transfer performance. At 90°, the magnetic field acts perpendicularly to the flow, which induces stronger flow damping via Lorentz forces, further reducing convective heat transport.

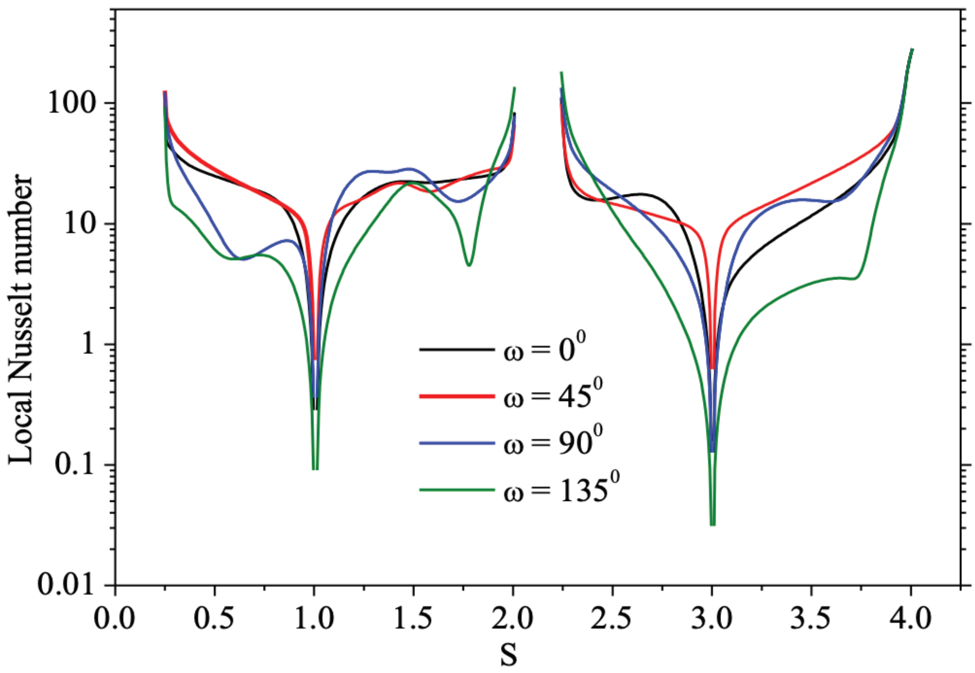

Figure 9. Magnetic field direction effects on the local Nusselt number for the configuration P_4 at Ha = 100, Re = 500 and φ = 2%.

In addition, Figure 10 shows the effect of the obstacle position in the ventilated cavity on the local Nusselt number evolution, for the angle ω = 45°. It is important to note that estimating the best configuration on the local Nusselt number is difficult and requires computing the average Nusselt number for all control parameters.

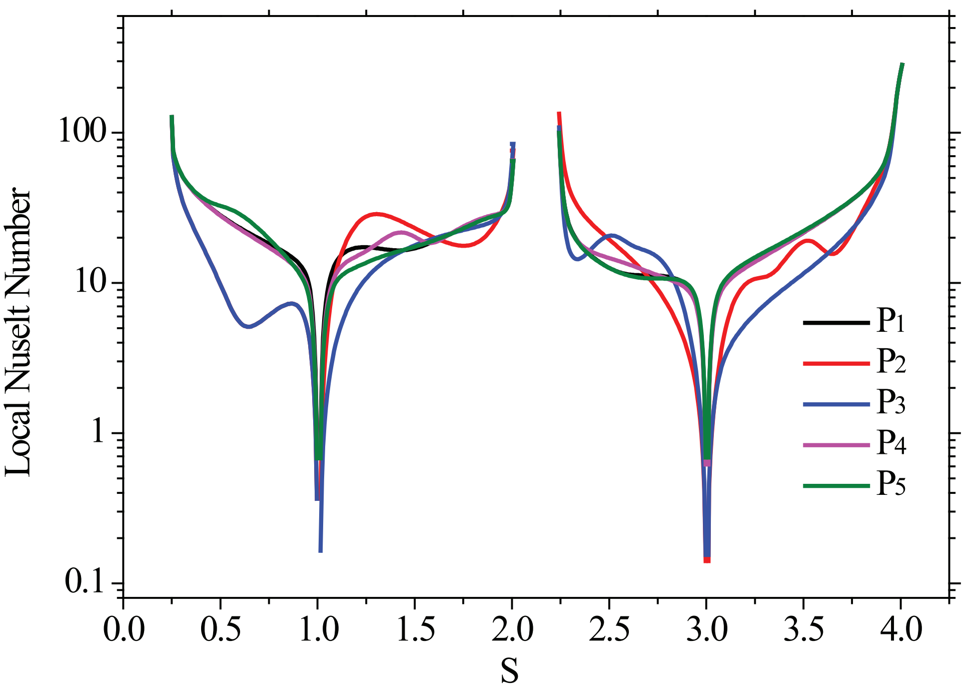

Figure 10. Obstacle positions effects on the local Nusselt number at Re = 500, Ha = 100, ω = 45°and φ = 2%.

Figures 11 and 12 illustrate the variation of the average Nusselt number as a function of Lorentz force intensity, obstacle position, and magnetic field direction for Reynolds numbers Re = 50 and Re = 500, respectively. The results indicate that the most effective heat transfer occurs for Re = 500. At Re = 50, we notice that the P_5 configuration is the optimal choice in the absence of a magnetic field. Indeed, in the presence of the magnetic field, we observe that increasing the Lorentz force intensity enhances the heat exchange rate for different angles of the applied magnetic field. Except when the angle is 135°, where the average Nusselt number decreases. For example, when the magnetic field is imposed in the horizontal direction (ω = 0°) at Ha = 100 for the P_4 configuration, the heat exchange rate is improved by about 17.25% compared to the case of no magnetic field. Thus, the choice of the optimal configuration depends on the intensity and the angle of the applied magnetic field. For Re = 500 (Fig. 12), we observe that the average Nusselt number decreases with increasing the magnetic field intensity in the relatively small Hartmann number and then increases to large values. In particular, for an angle equal to 45°, the average Nusselt number decreases until Ha = 30, after which it increases to reach a maximum at Ha equal to 100. For the P_4 configuration, we find that the average Nusselt number increases by 16.20% compared to the case of no magnetic field,when the cavity is subjected to a magnetic field in the direction ω = 45° with Ha = 100. When ω = 135°, the average Nusselt number is reduced with an increased in the magnitude of magnetic field for all arrangements.

The positioning of obstacles significantly impacts the heat transfer process under varying Reynolds and Hartmann numbers. At Re = 500, configurations such as P_4 demonstrate superior heat transfer efficiency due to optimal interaction between the flow dynamics and the imposed Lorentz forces. When the obstacle is placed at P_4, the thermal boundary layer is thinner, resulting in enhanced heat transfer. Furthermore, the intensity and direction of the magnetic field interact differently with obstacle positioning, altering the boundary layer's behavior and the flow structure within the cavity. These differences illustrate the influence of placing obstacles on the heat transfer performance.

The subfigure 12c shows that the heat transfer rate reaches its maximum when the obstacle is positioned at

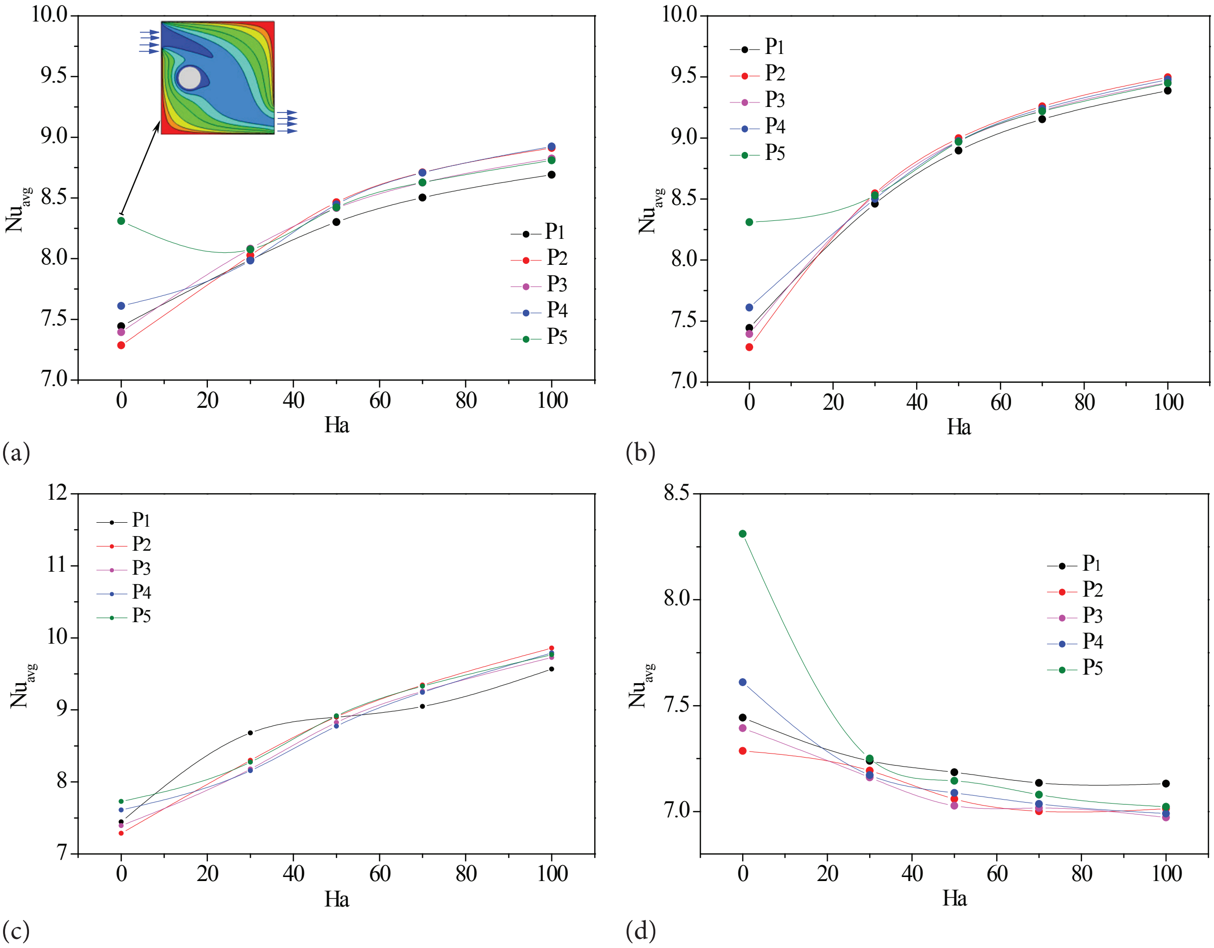

Figure 11. Effect of intensity and angle of magnetic field for different obstacle positions on the average Nusselt number at Re = 50 and φ = 2%: (a) ω = 0°, (b) ω = 45°, (c) ω = 90° and (d) ω = 135°.

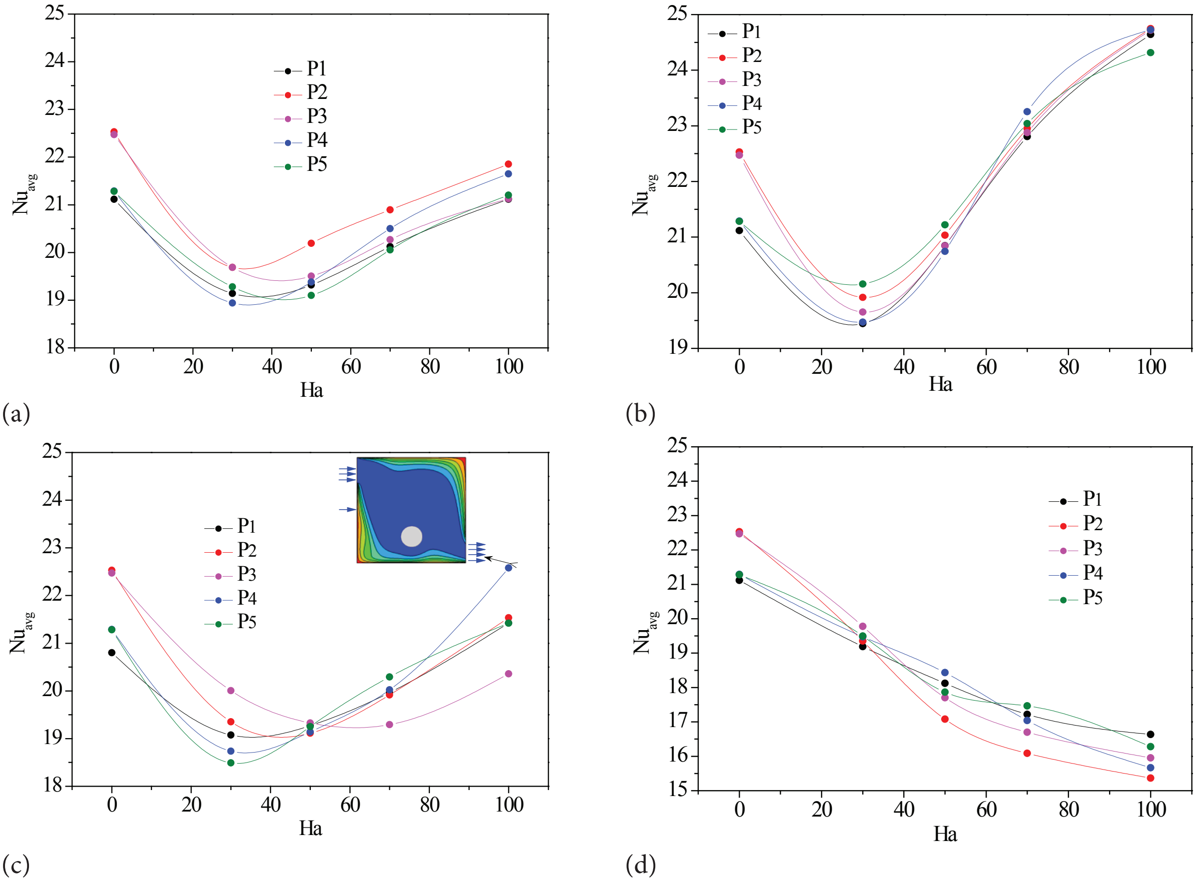

Figure 12. Effect of intensity and direction of magnetic field for different obstacle positions on the average Nusselt number at Re = 500 and φ = 2%: (a) ω = 0°, (b) ω = 45°, (c) ω = 90° and ω = 135°.

P_4 for Ha = 100. This result is primarily due to the limited development of the thermal boundary layer thickness, which is significantly thinner in this configuration compared to others. The reduced boundary layer thickness enhances the efficiency of heat transfer.

Pressure Drop

The pressure drop and thermal performance measurements inside the ventilated cavities are useful information. For this purpose, we plotted the evolution of the pressure drop for each cavity corresponding to the obstacle positionas a function of the variation of the Hartmann number and the angle of inclination of the applied magnetic through Figures 13 and 14, for Re = 50 and Re = 500, respectively. The results indicate that the pressure drop values for lower Reynolds numbers are higher than those for higher Reynolds numbers for all Hartmann numbers. Furthermore, we observe that the pressure drop increases with increasing Hartmann number for each Reynolds number. This is due to the effect of the Lorentz force, which causes a blockage of the fluid flow and consequently leads to the increase of the shear stresses. It can be noticed that the P_1 configuration gives themaximum pressure drop coefficient and that the P_4 and P_5 configurations give the minimum values of whatever the Reynolds number and the angle of the applied magnetic field. Moreover, it can be noted that the effect of changing the obstacle position on the pressure drop evolution is negligible for higher Hartmann numbers, except when the magnetic field angle is equal to 135°.

Nanoparticles Effects

Figure 15 shows the influence of nanoparticles water suspension on thermal performance. It is clear that only the presence of the nanoparticles has a positive influence, at low Reynolds number (Re = 50), for all different obstacle situations. Results show that the heat transfer rate increases when the volume fraction of graphene nanoplatelets is increased thanks to the higher thermal conductivity in comparison with base fluid, nevertheless this increase diminishes at high volume fractions due to a raise in viscosity resulting in which convection heat transfer decreases. The optimal nanoparticle volume fraction for heat transfer performance and manageable viscosity was observed at volume fractions of 1% and 2% for the configurations studied. Furthermore, the heat transfer rate is observed to be maximum at the greatest angle of the applied magnetic field (ω = 135°) for both Reynolds numbers. Moreover, the comparison between the different

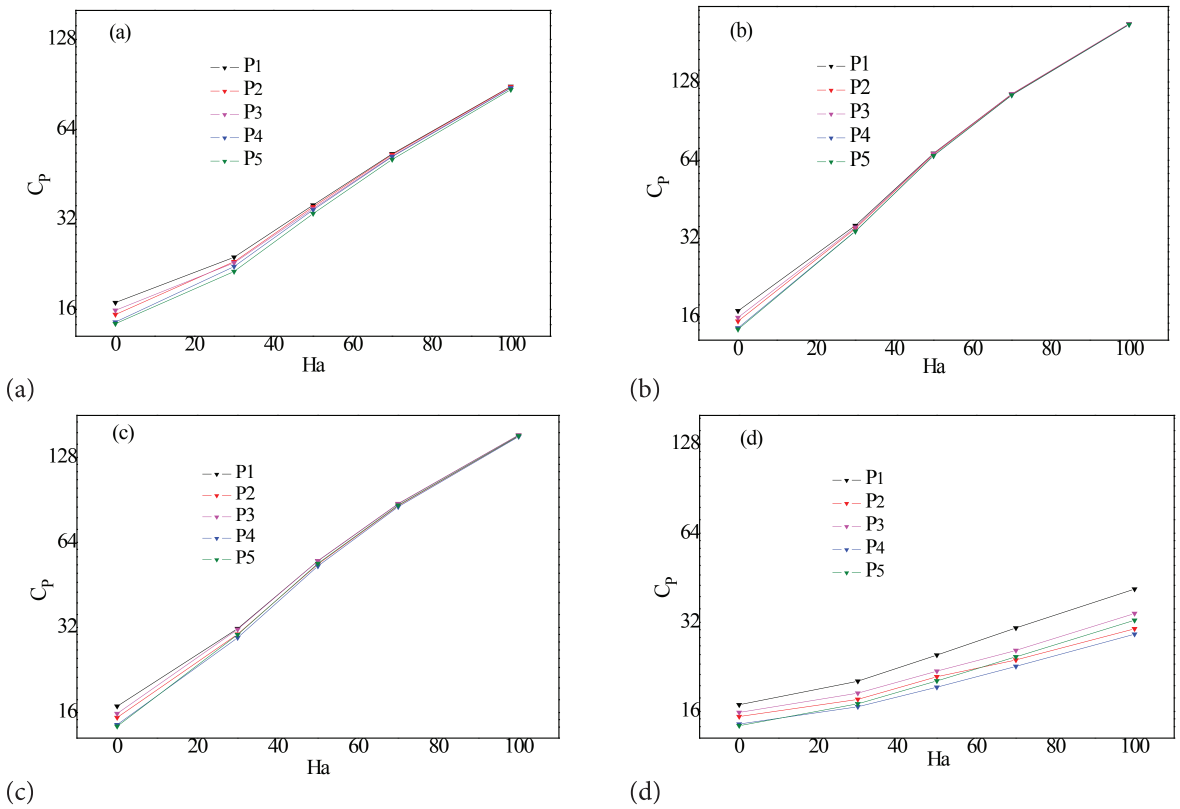

Figure 13. Effects of intensity and of magnetic field direction for different obstacle positions on the pressure drop at Re = 50 and φ = 2%: (a) ω = 0°, (b) ω = 45°, (c) ω = 90° and (d) ω = 135°.

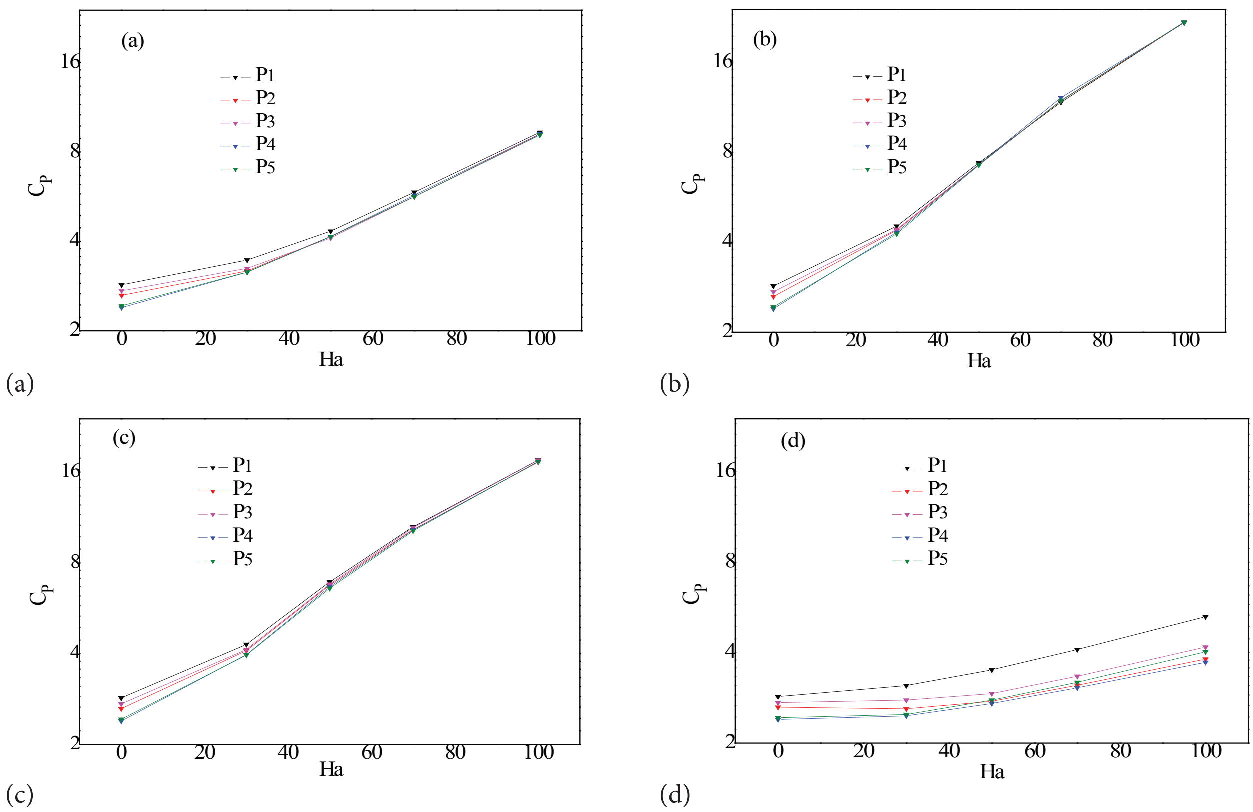

Figure 14. Effect of intensity and direction of magnetic field for different obstacle positions on the pressure drop at Re = 500 and φ = 2%: (a) ω = 0°, (b) ω = 45°, (c) ω = 90°and (d) ω = 135°.

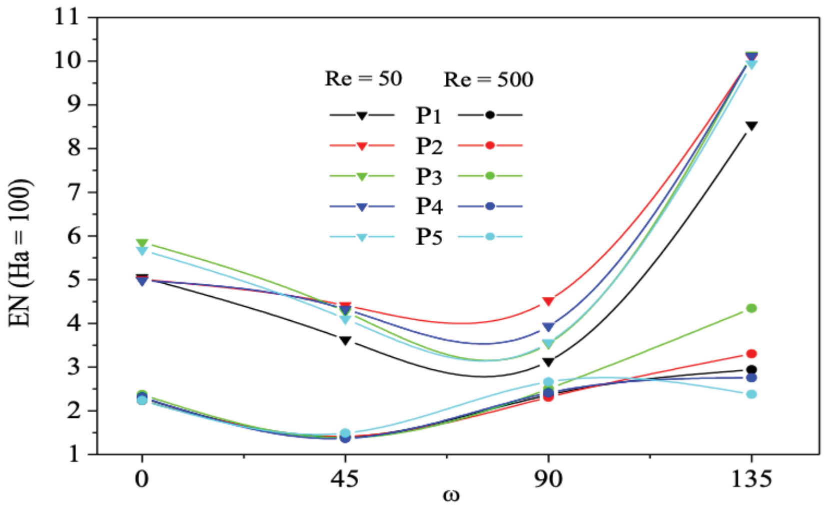

Figure 15. Nanoparticles effects on the heat transfer enhancement for all control parameters.

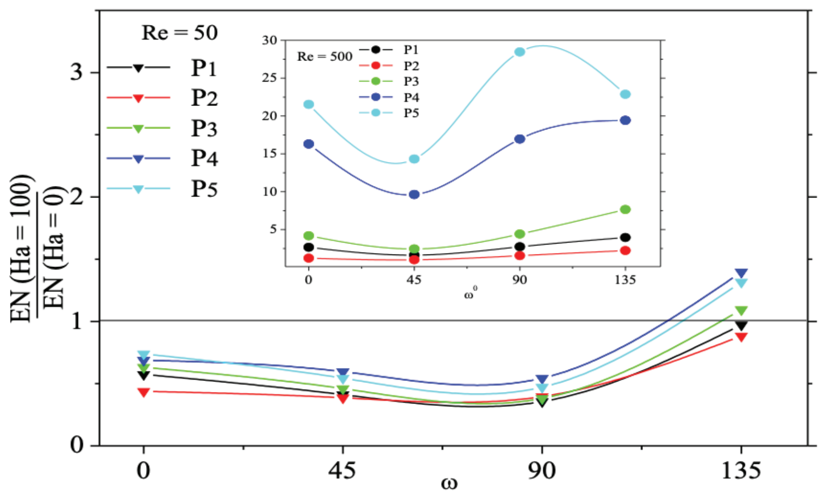

Figure 16. Nanoparticles effects for all control parameters.

configurations, in terms of the improvement brought by the addition of 2% of the nanoparticles, shows that one can choose an appropriate configuration for each angle of the applied magnetic field, in terms of the maximum enhancement brought by these CNT nanoparticles. For example, adding nanoparticles is advantageous for the case P_2 at the magnetic field angle is 135°. When the heat transfer enhancements of 3.30% and 10.09% for Re = 500 and Re = 50, respectively, are obtained compared to the base fluid, then it can be observed that presence of nanoparticles is favorable when conduction is more influential compare to convection mode.

Figure 16 shows the variation ratio between the heat transfer enhancement in the presence and the absence of the magnetic field as a function of the obstacle position and the magnetic field directions, for the two Reynolds numbers. The objective is to compare the impact of the addition of nanoparticles between the case of the absence and the case of the presence of the magnetic field. Thus, figure 16 indicates that the use of nanoparticles in the presence of the magnetic field in the case of Re = 50 is unfavorable for all configurations and the different magnetic field angles, except for configurations P_3, P_4, and P_5 when ω = 135°. In this case, the addition of nanoparticles proves advantageous under the influence of a magnetic field. However, for Re = 500, their benefit is observed only in configurations P_3, P_4, and P_5, regardless of the magnetic field's orientation.

CONCLUSION

In the present work, mixed convection inside a vented cavity with circular body filled by CNT-water nanofluid has been numerically explored in presence of magnetic field. Performance analysis was performed to investigate the influence of various parameters on heat transfer rates and pressure drop in order to find the best configuration. Novelties of the work are a detailed consideration of how the obstacle position together with the Lorentz force influence both flow dynamics and thermal aspects, which has not been thoroughly examined by previous studies. These findings also have implications on the design and optimization of efficient cooling or thermal-management system, such as electronics cooling and heat exchanger. Key points are as follows:

- Increasing the Reynolds number intensifies the hydrodynamic field and improves heat transfer, especially in the absence of the magnetic field.
- The introduction of the magnetic field weakens the hydrodynamic structure of the flow and causes a heat transfer in conduction mode.
- The pressure drop coefficient is a decreasing function with Reynolds number and an increasing function with Hartmann number.
- Obstacle position is significant on the heat transfer and the pressure drop in the absence of the magnetic field. Nevertheless, the presence of the magnetic field has a negligible effect on the pressure drop.
- The magnetic field direction and the Lorentz force intensity also play a big role in choosing the best configuration.
- The optimal configurations in the absence of a magnetic field are P_5 for Re = 50 and P_2 for Re = 500. Moreover, in the presence of the magnetic field for Ha = 100, we find that P_4 is the best for Re = 50 and ω = 90°. And the configuration P_5, for Re = 500 and ω = 45°.
- The use of nanoparticles is beneficial in conductive mode and for the low Reynolds number. In amagnetic field, it is advantageous for the high Reynolds number. In addition, the results show that the obstacle position is a predominant factor that disadvantages or favors the importance of the existence of these nanoparticles.

NOMENCLATURE

B	Magnetic field, T
Cp	Constant pressure specific heat, J kg^{-1} K^{-1}
g	Gravitational acceleration, ms^{-2}
Ha	Hartmann number, $Ha = \sqrt{\frac{\sigma B^2 L}{\mu}}$
k	Thermal conductivity, Wm^{-1} K^{-1}
Nu	Nusselt number
p	Pressure, Pa
Pr	Prandtl number
Re	Reynolds number
Ri	Richardson number
s	Distance along the walls, m
S	Dimensionless coordinate, S = sH^{-1}
T	Dimensional temperature, K
(u, v)	Velocity components in the x, y directions, m s^{-1}
(x, y)	Cartesian coordinates, m

Greek symbols

α	Thermal diffusivity, m^2 s^{-1}
b	Thermal expansion coefficient, K^{-1}
ρ	Density, kg m^{-3}
s	Electrical conductivity
ν	Kinematic viscosity, m^2 s^{-1}
μ	Dynamic viscosity, kg m^{-1} s^{-1}
θ	Dimensionless temperature
φ	Nanoparticle volume fraction

Superscript

EN	$\left[\frac{Nu_{avg}(\varphi=2\%)-Nu_{avg}(\varphi=0\%)}{Nu_{avg}(\varphi=0\%)}\right]\times 100$
avg	Average
bf	Base fluid
nf	Nanofluid
s	Solid particles

ACKNOWLEDGEMENTS

All authors contributed to the study conception and design. All authors read and approved the final manuscript.

AUTHORSHIP CONTRIBUTIONS

Authors equally contributed to this work.

DATA AVAILABILITY STATEMENT

The authors confirm that the data that supports the findings of this study are available within the article. Raw data that support the finding of this study are available from the corresponding author, upon reasonable request.

CONFLICT OF INTEREST

The author declared no potential conflicts of interest with respect to the research, authorship, and/or publication of this article.

ETHICS

There are no ethical issues with the publication of this manuscript.

STATEMENT ON THE USE OF ARTIFICIAL INTELLIGENCE

Artificial intelligence was not used in the preparation of the article.

FUNDING

This work was supported by the Directorate General for Scientific Research and Technological Development of Algeria (DGRSDT) with granted contracts (No. A16N01UN160420200007) and (No. A11N01UN440120220001).

REFERENCES

[1] Choi SU, Eastman JA. Enhancing thermal conductivity of fluids with nanoparticles. Argonne National Lab.(ANL), Argonne, IL (United States); 1995.

[2] Kakaç S, Pramuanjaroenkij A. Review of convective heat transfer enhancement with nanofluids. Int J Heat Mass Transf 2009;52(13-14):3187–3196. [CrossRef]

[3] Saidur R, Leong K, Mohammed HA. A review on applications and challenges of nanofluids. Renew Sustain Energy Rev 2011;15(3):1646–1668. [CrossRef]

[4] Vanaki SM, Ganesan P, Mohammed HA. Numerical study of convective heat transfer of nanofluids: A review. Renew Sustain Energy Rev 2016;54:1212–1239. [CrossRef]

[5] Zeghbid I, Bessaïh R. Mixed convection and entropy generation in a square cavity using nanofluids. Thermophys Aeromechanics 2018;25(2):245–256. [CrossRef]

[6] Ebrahimnia-Bajestan E, Niazmand H, Duangthongsuk W, Wongwises S. Numerical investigation of effective parameters in convective heat transfer of nanofluids flowing under a laminar flow regime. Int J Heat Mass Transf 2011;54(19-20):4376–4388. [CrossRef]

[7] Li Y, Tung S, Schneider E, Xi S. A review on development of nanofluid preparation and characterization. Powder Technol 2009;196(2):89–101. [CrossRef]

[8] Ouyahia SE, Benkahla YK, Labsi N. Numerical study of the hydrodynamic and thermal proprieties of titanium dioxide nanofluids trapped in a triangular geometry. Arab J Sci Eng 2016;41:1995–2009. [CrossRef]

[9] Oztop HF, Abu-Nada E. Numerical study of natural convection in partially heated rectangular enclosures filled with nanofluids. Int J Heat Fluid Flow 2008;29(5):1326–1336. [CrossRef]

[10] Sundar LS, Singh MK. Convective heat transfer and friction factor correlations of nanofluid in a tube and with inserts: A review. Renew Sustain Energy Rev 2013;20:23–35. [CrossRef]

[11] Yu W, France DM, Choi SU, Routbort JL. Review and Assessment of Nanofluid Technology for Transportation and Other Applications. Argonne National Lab.(ANL), Argonne, IL (United States); 2007.

[12] Godson L, Raja B, Mohan Lal D, Wongwises S. Convective heat transfer characteristics of silver-water nanofluid under laminar and turbulent flow conditions. Int Commun Heat Mass Transf 2012;39(1):92-97. [CrossRef]

[13] Kumar PM, Kumar J, Tamilarasan R, Nathan SS, Suresh S. Heat transfer enhancement and pressure drop analysis in a helically coiled tube using Al2O3/water nanofluid. J Mech Sci Technol 2014;28:1841–1847. [CrossRef]

[14] Palanisamy K, Kumar PM. Experimental investigation on convective heat transfer and pressure drop of cone helically coiled tube heat exchanger using carbon nanotubes/water nanofluids. Heliyon 2019;5(5):e01705. [CrossRef]

[15] Garoosi F, Rohani B, Rashidi MM. Two-phase mixture modeling of mixed convection of nanofluids in a square cavity with internal and external heating. Powder Technol 2015;275:304–321. [CrossRef]

[16] Hussain S, Öztop H, Jamal M, Hamdeh N. Double diffusive nanofluid flow in a duct with cavity heated from below. Int J Mech Sci 2017;131:535–545. [CrossRef]

[17] Jalali H, Abbassi H. Numerical Investigation of Heat Transfer by Al2O3–water Nanofluid in Square Cavity. Springer; 2012. p. 1129–1138. [CrossRef]

[18] Khoshvaght-Aliabadi M, Arani-Lahtari Z. Proposing new configurations for twisted square channel (TSC): Nanofluid as working fluid. Appl Therm Eng 2016;108:709–719. [CrossRef]

[19] House JM, Beckermann C, Smith TF. Effect of a centered conducting body on natural convection heat transfer in an enclosure. Numer Heat Transf 1990;18(2):213–225. [CrossRef]

[20] Bhave P, Narasimhan A, Rees D. Natural convection heat transfer enhancement using adiabatic block: Optimal block size and Prandtl number effect. Int J Heat Mass Transf 2006;49(21-22):3807–3818. [CrossRef]

[21] Raji A, Hasnaoui M, Naïmi M, Slimani K, Ouazzani M. Effect of the subdivision of an obstacle on the natural convection heat transfer in a square cavity. Comput Fluids 2012;68:1–15. [CrossRef]

[22] Mahfoud B. Natural convection of a nanofluid in a conical container. J Therm Eng 2018;4(1):1713–1723. [CrossRef]

[23] Belhadj A. Numerical investigation of forced convection of nanofluid in microchannels heat sinks. J Therm Eng 2018;4(5):2263–2273. [CrossRef]

[24] Pandey S, Park YG, Ha MY. An exhaustive review of studies on natural convection in enclosures with and without internal bodies of various shapes. Int J Heat Mass Transf 2019;138:762–795. [CrossRef]

[25] Sharma B, Kumar B, Barman RN. Numerical investigation of Cu-water nanofluid in a differentially heated square cavity with conducting solid square cylinder at center. Int J Heat Technol 2018;36(2):714–722. [CrossRef]

[26] Mahmoodi M, Sebdani SM. Natural convection in a square cavity containing a nanofluid and an adiabatic square block at the center. Superlattices Microstruct 2012;52(2):261–275. [CrossRef]

[27] Park Y, Ha M, Park J. Natural convection in a square enclosure with four circular cylinders positioned at different rectangular locations. Int J Heat Mass Transf 2015;81:490–511. [CrossRef]
[28] Soomro FA, Hammouch Z. Heat transfer analysis of CuO-water enclosed in a partially heated rhombus with heated square obstacle. Int J Heat Mass Transf 2018;118:773–784. [CrossRef]
[29] Sourtiji E, Gorji-Bandpy M, Ganji D, Hosseinizadeh S. Numerical analysis of mixed convection heat transfer of Al2O3-water nanofluid in a ventilated cavity considering different positions of the outlet port. Powder Technol 2014;262:71–81. [CrossRef]
[30] Benzema M, Benkahla YK, Labsi N, Brunier E, Ouyahia SE. Numerical mixed convection heat transfer analysis in a ventilated irregular enclosure crossed by Cu–water nanofluid. Arab J Sci Eng 2017;42:4575–4586. [CrossRef]
[31] Milani Shirvan K, Mamourian M, Ellahi R. Numerical investigation and optimization of mixed convection in ventilated square cavity filled with nanofluid of different inlet and outlet port. Int J Numer Methods Heat Fluid Flow 2017;27(9):2053–2069. [CrossRef]
[32] Rahman MM, Alim MA, Saha S, Chowdhury M. A numerical study of mixed convection in a square cavity with a heat conducting square cylinder at different locations. J Mech Eng 2008;39(2):78–85. [CrossRef]
[33] Rahman MM, Parvin S, Rahim N, Islam M, Saidur R, Hasanuzzaman M. Effects of Reynolds and Prandtl number on mixed convection in a ventilated cavity with a heat-generating solid circular block. Appl Math Model 2012;36(5):2056–2066. [CrossRef]
[34] M'hamed B, Sidik NAC, Yazid MNAWM, Mamat R, Najafi G, Kefayati G. A review on why researchers apply external magnetic field on nanofluids. Int Commun Heat Mass Transf 2016;78:60–67. [CrossRef]
[35] Rudraiah N, Barron R, Venkatachalappa M, Subbaraya C. Effect of a magnetic field on free convection in a rectangular enclosure. Int J Eng Sci 1995;33(8):1075–1084. [CrossRef]
[36] Yu P, Qiu J, Qin Q, Tian ZF. Numerical investigation of natural convection in a rectangular cavity under different directions of uniform magnetic field. Int J Heat Mass Transf 2013;67:1131–1144. [CrossRef]
[37] Selimefendigil F, Öztop HF. Natural convection and entropy generation of nanofluid filled cavity having different shaped obstacles under the influence of magnetic field and internal heat generation. J Taiwan Inst Chem Eng 2015;56:42–56. [CrossRef]
[38] Sheikholeslami M, Gerdroodbary MB, Shafee A, Tlili I. Hybrid nanoparticles dispersion into water inside a porous wavy tank involving magnetic force. J Therm Anal Calorim 2020;141:1993–1999. [CrossRef]
[39] Manh TD, Bahramkhoo M, Barzegar Gerdroodbary M, Nam ND, Tlili I. Investigation of nanomaterial flow through non-parallel plates. J Therm Anal Calorim 2021;143:3867–3875. [CrossRef]
[40] Tlili I, Moradi R, Barzegar Gerdroodbary M. Transient nanofluid squeezing cooling process using aluminum oxide nanoparticle. Int J Mod Phys C 2019;30(11):1950078. [CrossRef]
[41] Sheikholeslami M, Bandpy MG, Ellahi R, Zeeshan A. Simulation of MHD CuO–water nanofluid flow and convective heat transfer considering Lorentz forces. J Magn Magn Mater 2014;369:69–80. [CrossRef]
[42] Mehrez Z, El Cafsi A, Belghith A, Le Quere P. MHD effects on heat transfer and entropy generation of nanofluid flow in an open cavity. J Magn Magn Mater 2015;374:214–224. [CrossRef]
[43] Al-Rashed AA, Kolsi L, Kalidasan K, Malekshah EH, Borjini MN, Kanna PR. Second law analysis of natural convection in a CNT-water nanofluid filled inclined 3D cavity with incorporated Ahmed body. Int J Mech Sci 2017;130:399–415. [CrossRef]
[44] Moderres M, Boutra A, Kherroubi S, Oztop HF, Benkahla YK. Magnetohydrodynamic (MHD) natural convection flow of titanium dioxide nanofluid inside 3D cavity containing a hot block: Comparative with 2D cavity. J Nanofluids 2023;12(5):1298–1319. [CrossRef]
[45] Mehmood K, Hussain S, Sagheer M. Mixed convection in alumina-water nanofluid filled lid-driven square cavity with an isothermally heated square blockage inside with magnetic field effect: Introduction. Int J Heat Mass Transf 2017;109:397–409. [CrossRef]
[46] Javed T, Siddiqui M, Mehmood Z. MHD natural convective flow through a porous medium in a square cavity filled with liquid gallium. Thermophys Aeromechanics 2018;25:405–420. [CrossRef]
[47] Barzegar Gerdroodbary M. Application of neural network on heat transfer enhancement of magnetohydrodynamic nanofluid. Heat Transf Asian Res 2020;49(1):197–212. [CrossRef]
[48] Panigrahi L, Panda J, Kumar D, Sahoo SS. Analytical investigation of polar fluid flow with induced magnetic field in concentric annular region. Heat Transf 2020;49(6):3943–3957. [CrossRef]
[49] Panigrahi L, Panda J, Sahoo SS. Unsteady heat transfer and entropy generation study on viscoelastic fluid flow coupled with induced magnetic field. Iran J Sci Technol Trans A Sci 2021;45(5):1699–1710. [CrossRef]
[50] Benzema M, Benkahla YK, Labsi N, Ouyahia SE, El Ganaoui M. Second law analysis of MHD mixed convection heat transfer in a vented irregular cavity filled with Ag–MgO/water hybrid nanofluid. J Therm Anal Calorim 2019;137:1113–1132. [CrossRef]

[51] Kherroubi S, Ragui K, Bensaci A, Labsi N, Boutra A, Benkahla YK. Effect of the second outlet location and the applied magnetic field within a ventilated cubic cavity crossed by a nanofluid on mixed convection mode: Best configurations. J Therm Anal Calorim 2020;139:2243–2264. [CrossRef]

[52] Mishra M, Panda J, Kumar D, Sahoo SS. Thermal radiation and Soret effects on boundary layer flow past a vertical surface embedded in porous medium with induced magnetic field with reference to aluminum industry. J Therm Anal Calorim 2022;147(23):13829–13845. [CrossRef]

[53] Man Y, Gerdroodbary MB. Influence of Lorentz forces on forced convection of nanofluid in a porous enclosure. J Porous Media 2024;27(8). [CrossRef]

[54] Mishra M, Panda J, Sahoo SS. Investigations concerning the effects of thermal radiation, induced magnetic field, and chemical reaction on MHD flow through a permeable medium. Int J Mod Phys B 2024;38(02):2450030. [CrossRef]

[55] Gerdroodbary MB, Jafaryar M, Sheikholeslami M, Amini Y. The efficacy of magnetic force on thermal performance of ferrofluid in a screw tube. Case Stud Therm Eng 2023;49:103187. [CrossRef]

[56] Kefayati GR, Tang H. MHD mixed convection of viscoplastic fluids in different aspect ratios of a lid-driven cavity using LBM. Int J Heat Mass Transf 2018;124:344–367. [CrossRef]

[57] Yu P, Tian Z. Comparison of the simplified and full MHD models for laminar incompressible flow past a circular cylinder. Appl Math Model 2017;41:143–163. [CrossRef]

[58] Bhattacharya P, Samanta A, Chakraborty S. Numerical study of conjugate heat transfer in rectangular microchannel heat sink with Al2O3/H2O nanofluid. Heat Mass Transf 2009;45:1323–1333. [CrossRef]

[59] Patankar S. Numerical Heat Transfer and Fluid Flow. Boca Raton: CRC Press; 2018. [CrossRef]

[60] Krane R. Some detailed field measurements for a natural convection flow in a vertical square enclosure. In: Proceedings of the 8th International Heat Transfer Conference; 1986 Aug 17-22; San Francisco, CA. Hemisphere Publishing Corp.; 1986. p. 323–329.